Chemical Engineering Journal 152 (2009) 480–491

Contents lists available at ScienceDirect

Chemical Engineering Journal

journal homepage: www.elsevier.com/locate/cej

Nanostructured hydrous titanium(IV) oxide: Synthesis, characterization and Ni(II) adsorption behavior

Sushanta Debnath, Uday Chand Ghosh*

Department of Chemistry, Presidency College, 86/1 College Street, Kolkata 700073, India

ARTICLE INFO

Article history:
Received 24 December 2008
Received in revised form 27 April 2009
Accepted 8 May 2009

Keywords:
Nano-titanium(IV) oxide
Characterization
Adsorption–desorption
Kinetics
Nickel(II)
Thermodynamics

ABSTRACT

The synthetic oxide was characterized as hydrated and agglomerated nanocrystallite (11–13 nm) titanium(IV) oxide (NHTO), which was used for Ni(II) adsorption from aqueous solution. The variable parameters investigated were the effects of pH, contact time, metal concentration and temperature on reaction. The optimum pH fixed was 5.0 (±0.1) for Ni(II) adsorption. The kinetic data described the pseudo-first order equation well and, film diffusion governed the reaction. The Redlich–Peterson equation described well the equilibrium isotherm data of all temperatures. The Fe(III) showed negative influence on Ni(II) adsorption. The negative Gibbs free energy ($-\Delta G^{\circ}$ = 13.90–16.30 kJ mol^{-1}) and positive enthalpy change ($+\Delta H^{\circ}$ = 6.15 kJ mol^{-1}) indicated spontaneous and endothermic nature of the reaction, respectively, and took place with increasing entropy (ΔS° = +0.07 kJ mol^{-1} K^{-1}). The mean energy of adsorption (E_{DR} = 13.25–16.35 kJ mol^{-1} at T = 288–328 K) predicted physisorption nature of Ni(II) on NHTO. The dilute (0.1 M) mineral acids desorbed 95–98% of adsorbed metal from the NHTO surface.

1. Introduction

Titanium(IV) oxide (TiO_2) has wide applications and investigated in solar energy conversion [1], photocatalyst [2], sensors [3], photochromic devices [4]. Carp et al. [5] and Li et al. [6] had applied TiO_2 for polluted air and wastewater purifications. Hydrated TiO_2 had been studied for arsenic [7], lead [8] and chromium [9,10] removal from natural and industrial wastewater. Some nanostructure materials had been used for investigating the quality upgradation of contaminated water [11–13]. Nanostructured TiO_2 has gained special attention for photocatalytic property for the treatment of wastewater contaminated with phenolic compound [14] and organic dye [15–19]. However, the use of nano-TiO_2 for heavy metal contaminated water treatment is found not frequent in the literature. Heavy metal ions, if present in high level in water, cause the adverse effect on the health of animals, aquatic lives, microorganisms and human beings. They are readily accumulated by the marine biomass and enter into the human food chains, presenting a high health risk to the consumers [20]. Ni(II) is one of the heavy metal ion which is non-biodegradable and that causes dermatitis and allergic sensitization [21]. It may be conducive for the cancer of lungs, nose and bones. The sources of Ni(II) contamination to water are mainly the industrial processes such as electroplating, batteries manufacturing, mining, metal finishing and forging. In 1984, United State Environmental Protection Agency (USEPA) [22] fixed up that the maximum permissible concentration level (MACL) of Ni(II) is 4.1 and 0.1 mg L^{-1}, respectively, for the wastewater discharge and drinking water. Thus, researchers had paid their attention in reducing Ni(II) below MACL from the contaminated water using adsorbents, viz., sea weeds [23], crab shell [24], dried aerobic activated sludge [25], activated carbon prepared from almond husk [26], spent animal bones [27], waste of tea factory [28], raw kaolinite [29], sodium and calcium bentonite [30], kaolinite and montmorillonite with their modified forms [31,32], bagasse fly ash [33], peat [34] and granular activated carbon with modified form [35]. Despite less costing of the materials, low adsorption capacities or efficiencies of many of the materials limited their application. Recent trends show the use of synthetic nanostructured material for environmental remediation. This encouraged us to synthesize nanoparticle agglomerate of TiO_2 for application as the scavenger of toxic metal ions from the contaminated water.

The methods available in literatures for nano-TiO_2 synthesis are generalized as the (i) alkoxide based sol–gel method [15,36–38], (ii) thermal hydrolysis of $TiCl_4$ in n-propanol and water mixed solvent [39], (iii) thermal hydrolysis of $Ti(SO_4)_2$ in n-propanol and water mixed solvent [40], (iv) hydrolysis of $TiCl_4$ with NH_4OH in ice-water bath in the presence of $(NH_4)_2SO_4$ + HCl [41] and (v) thermo hydrolysis of $TiCl_4$ [42]. The methods noted above for the nano-TiO_2 synthesis were to apply the products as photooxidation catalyst, photoluminescence, sensors, etc. The products did not used for the treatment of metal contaminated water presumably due to poor adsorption capacity.

* Corresponding author. Tel.: +91 33 2241 3893; fax: +91 33 2241 3893.
E-mail address: ucghosh@yahoo.co.in (U.C. Ghosh).

1385-8947/$ – see front matter © 2009 Elsevier B.V. All rights reserved.
doi:10.1016/j.cej.2009.05.021

The present communication herein reports (i) the synthesis and characterization of nanostructured hydrous TiO_2 (NHTO), and (ii) the adsorption of Ni(II) by NHTO for removal from the aqueous solution.

2. Materials and methods

2.1. Reagents

Titanium(IV) tetrachloride used for the synthesis of NHTO was of reagent grade (Spectrochem, India). Nickel (II) chloride used for the preparation of stock (1000 mg Ni(II) L^{-1}) solution was guaranteed reagent (G.R.) of E. Merck (India). The metal solution of desired concentrations for working was prepared from the measured stock by appropriate dilution with distilled water. Dimethylglyoxime (DMG) (analytical reagent, BDH, England) and liquid Br_2 (G.R., E. Merck, India) were used for the colorimetric analysis of Ni(II). Other reagents used were of guaranteed/laboratory reagent grade.

2.2. Analytical instruments

The analytical instruments availed for collections of data were (i) ELICO pH meter (model: LI 127, India) for pH analysis, (ii) Phillips X-ray diffractometer for the X-ray diffraction (XRD) pattern, (iii) Setaram analyzer for thermogravimetric (TG) and differential thermal (DT) analyses in an argon atmosphere at a heating rate of 20 °C/min over a range of temperature 30–1000 °C, (iv) Föurier transform infra red (FTIR) spectrophotometer (Jasco 680 plus) for FTIR spectra, (v) FEI high resolution transmission electron microscope (HRTEM) (model: Tecnai S Twin) for the image of the material for the particle size, (vi) scanning electron microscope (SEM) (Tescan Vega, UK) for the surface morphology of the material and (vii) UV–vis spectrophotometer (Hitachi model: U 3210) for colorimetric analysis of nickel(II).

2.3. Analysis of Ni(II)

The metal ion in solution was analyzed by a color developing method using a spectrophotometer [43]. An aliquot of the test solution was taken with 10 mL of 0.5 M HCl into a 25-mL volumetric flask. Diluting to about 20 mL with distilled water, 1 mL saturated Br_2-water, 2 mL ammonia solution (1:1) and 1 mL DMG (1% in ethanol) reagent were added and mixed well. The volume was filled in with distilled water up to the mark of the flask. The absorbance of developed red to orange solution was measured at 445 nm against reagent blank after 5 min of reagent mixing. The Ni(II) concentration was calculated from the Beer's law curve. While the effect of diverse ions is observed, the nickel was initially precipitated using DMG in ammonia solution and extracted in 10 mL chloroform. The chloroform extract was returned back to ionic state using 0.5 M HCl, and the absorbance was determined for nickel concentration.

2.4. Preparation of NHTO

Liquid titanium(IV) chloride was injected (30 mL $TiCl_4$ per L) slowly into the distilled water with constant mechanical agitation (1000 rpm). The curd-like precipitate including liquid was treated with ammonia (0.1 M) with agitation till the pH of supernatant was 7.5 (±0.1). The precipitate, being aged with the mother liquid for 6 days, was filtered and washed thrice with deionised water. The white product was dried in an air-oven 70 (±5)°C, and treated with cold water. This material after drying in air was ground and screened through a set of sieves for the particles agglomerate of size ranged in 0.29–0.36 mm for conducting adsorption experiments.

2.5. Specific surface area of NHTO

Specific surface area was analyzed by the Sear's method [44]. To the suspension of powdered NHTO (1.50 g) in water, dilute HCl was added to adjust pH between 3.0 and 3.5. To this sol, 30 g of sodium chloride were added and, diluted to 150 mL with distilled water. The titration was carried out slowly using 0.1N NaOH with continuous monitoring of pH. The volume (V) of 0.1N NaOH solution required to increase pH of the suspension from 4.0 to a steady value of 9.0 was recorded. The specific surface area (S) was calculated by the formulation, $S = 32V - 25$ [44].

2.6. Determination of point of zero charge (pzc) of NHTO

The pzc of the material was analyzed according to the method described by Babic et al. [45]. Here, a series of 0.1N NaCl solutions were prepared at separate initial pH (pH_i) 1.0–10.0. 50 mL aliquot of each solution was added with 0.1 g NHTO into 10 separate 250 mL PET bottles and agitated (300 ± 10 rpm) using an orbital shaker till the pH reading was same of two successive measurements. The equilibrium solution pH (pH_f) was noted, and plotted against initial pH (pH_i). The horizontal portion of the pH_i versus pH_f plot with the pH_i axis is the pzc range of the adsorbent [45].

2.7. Adsorption experiments

The adsorbent material of amount 0.1 g was placed in a 250-mL PET bottle in which 50 mL solution of Ni(II) of desired initial concentration (C_0, mg L^{-1}) was added and, the mixture was shaken by a thermostat rotary shaker using agitation speed of 300 ± 5 rpm for the required contact time at some definite temperatures, T (±1) °C. The mixture was then centrifuged, and the concentration at time, t (C_t, mg L^{-1}) or at equilibrium (C_e, mg L^{-1}) of Ni(II) in centrifuged solution was analyzed [43].

The amount of Ni(II) adsorbed per unit mass of the adsorbent (q_{ad}) was calculated by Eq. (1).

$$q_{ad} = \frac{q_i - q_r}{m} \quad (1)$$

where q_{ad} (mg g^{-1}) becomes q_e or q_t at equilibrium or at time t. q_i and q_r are the initial and the residual amount (mg) of Ni(II), respectively, added and remained in solution. 'm' is the mass (g) of the adsorbent added for the experiments.

The effect of pH_i on Ni(II) adsorption was carried out in pH_i ranged between 2.0 and 10.0 at T = 30 °C by the procedure described above taking Ni(II) solution of C_0 = 10.0 mg L^{-1}, and agitation time for a duration of 1 h. The same set of experiments was also conducted at identical pH condition without putting NHTO. The centrifuged solutions were analyzed for Ni(II) concentrations [43] and pH_f.

The kinetic experiments were carried out taking the Ni(II) solution of desired C_0 at pH_i 5.0 ± 0.1 and at separate T = 15, 30 and 45 °C. To the 500 mL of metal solution (C_0 = 10.0, 30.0 and 50.0 mg L^{-1}) in 1.0 L beaker in a thermostat, 1.0 g NHTO was placed and agitated at a speed of 300 (±5) rpm. The reaction mixture was sampled (1.0 mL) at an interval of pre-fixed time from t = 0, and centrifuged. The concentration of Ni(II) at a time t (C_t, mg L^{-1}) was analyzed in centrifuged solution for the calculation of adsorption capacity, q_t (mg g^{-1}).

The batch equilibrium experiments were conducted by the procedure described earlier using Ni(II) solution of C_0 ranged in 10.0–150.0 mg L^{-1}. The agitation (300 ± 5 rpm) was continued for 45 min in a thermostat shaker separately at T = 15, 30 and 45 °C. The centrifuged solutions were analyzed for the residual Ni(II) concentration (C_e, mg L^{-1}) by the standard method [43] and, the q_e was calculated.

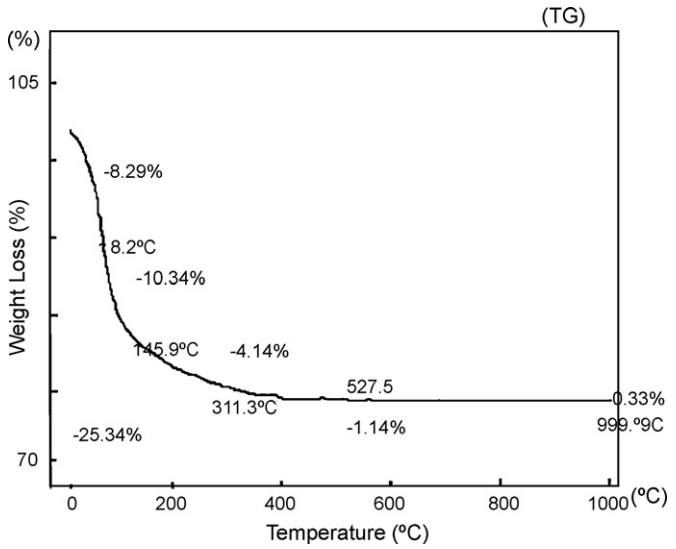

Fig. 1. The thermo gravimetric (TG) spectrum of NHTO in the temperature ranged in 30–1000 °C.

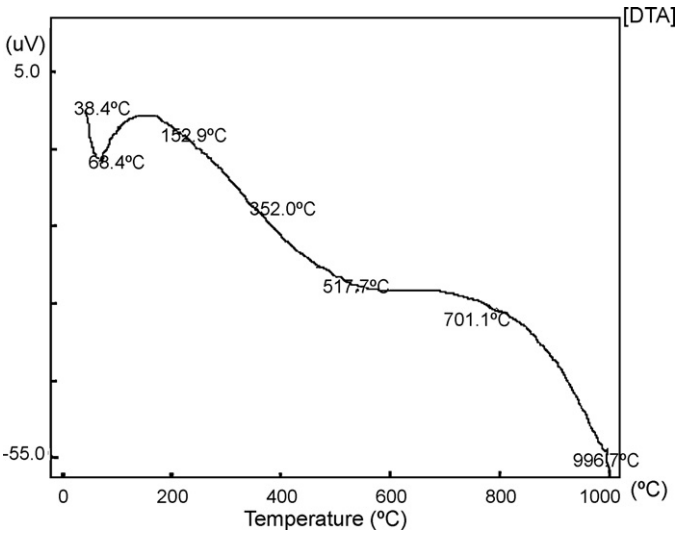

Fig. 2. The differential thermal (DT) spectrum of NHTO in the temperature ranged in 30–1000 °C.

2.8. Desorption experiment

For the desorption experiments, 2.0 g NHTO was taken with 200 mL of 1000 mg L^{-1} Ni(II) solution at pH_i 5.0 ± 0.1 into a said PET bottle. The reaction mixture was agitated (300 ± 5 rpm) at T = 30 °C for 45 min. The solid (Ni-NHTO, q_e = 26.90 mg Ni g^{-1}) material was separated from the solution by centrifugation, and washed with distilled water. One-half portion of Ni-NHTO was dried at 60 (±5) °C (sample: T-1) and remaining half portion was dried at 150 (±5) °C (sample: T-2). Desorption experiments were conducted using the samples T-1 and T-2 separately. Here, 0.1 g of each sample (26.9 mg Ni g^{-1}) was taken separately with 50 mL of regenerating solution (dilute mineral acids/some salts solutions) in PET bottles, and agitated (300 ± 5 rpm) for 45 min at T = 30 °C. The liquid was separated from the solid by centrifugation and analyzed for Ni(II) for calculating the desorption percentage of Ni(II).

3. Results and discussion

3.1. Physicochemical characterization

The TG spectrum (Fig. 1) of NHTO showed that the loss of weight by 8.29% took place at a temperature below 100 °C. The endothermic peak of DT spectrum at 68.4 °C (Fig. 2) supported the loss of weight. This weight loss is due to the loss of physically attached water molecules. The additional 12.25% weight loss was found in TG spectrum which corresponds to the broad exothermic DT peak between 68.4 and 200 °C. This has been attributed to the chemical change of synthetic oxide due to polymerization with loss of water from the hydroxyl groups. The broad exothermic DT peak at the drying temperature between 600 and 800 °C had indicated the transition of phase of the material. Thus, the synthetic material was hydrated, and stable up to the temperature below 600 °C. The absorbance band at wave number ranged between 3100 and 3500 cm^{-1} in the FTIR spectrum (Fig. 3) had also confirmed the hydrated nature of synthetic oxide. The powder XRD pattern (Fig. 4) of the material taken at the start and the end diffraction angle (°2θ) values between 10 and 80 showed eight peaks at 12.64°, 25.36°, 30.48°, 38.13°, 47.95°, 54.19°, 63.15° and 75.64°. The mineralogical analysis suggested that the synthetic material was of mixed phases, viz., brookite, anatase and rutile with predominance of anatase phase. It was found to be similar to the result that had been reported by Paola et al. [42] but different from Zhang et al. [41] and Kanna

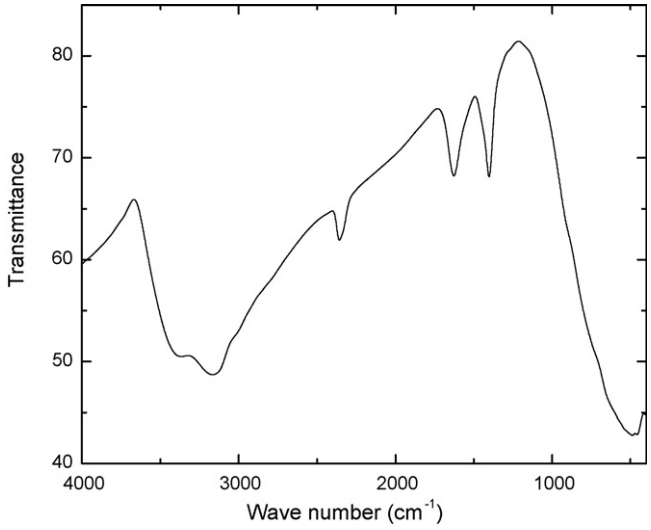

Fig. 3. The Föurier transform infra red (FTIR) spectrum of NHTO.

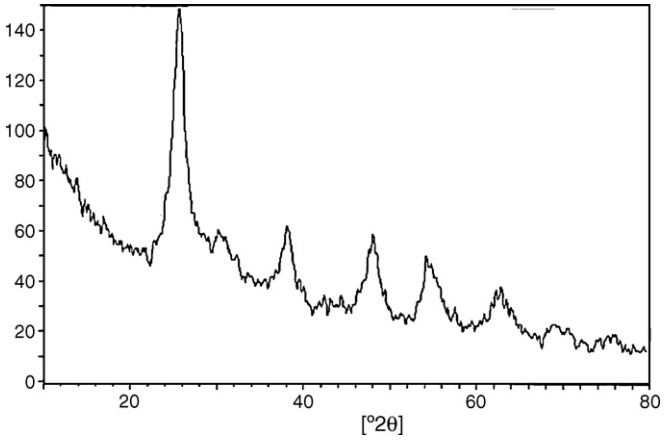

Fig. 4. The powder X-ray diffraction (XRD) pattern of NHTO.

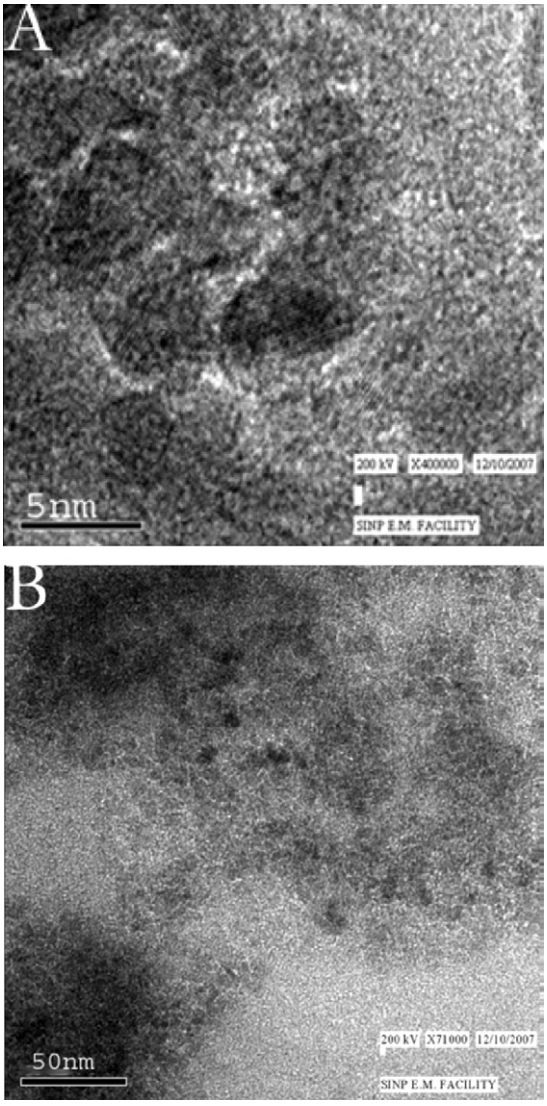

Fig. 5. High resolution transmission electron microscopic (HR-TEM) images at (a) 40×10^4 times magnification (10 nm scale) and (b) 71×10^3 times magnification (50 nm scale) of NHTO.

and Wongnawa [15]. Additionally, the XRD peak pattern (Fig. 4) suggested that the synthetic material was crystalline in nature. The crystallite size of the sample as calculated by the Scherer's equation [46] using the XRD peak data was ranged in ~19–23 nm while that was 11–13 nm from the analysis of TEM image (Fig. 5) of NHTO. The fingerprint like appearance in TEM image had also supported the presence of crystalline phase in the material. The SEM image (figure omitted) suggested irregular surface morphology of agglomerated particles of the material. The specific surface area and pH_{pzc} of NHTO as analyzed were found to be $663.0 \pm 5.5\ m^2\ g^{-1}$ and 6.5 ± 0.3, respectively. Table 1 summaries the parameters analyzed for the characterization of the synthetic oxide.

Table 1
Some parameters analyzed for the characterization of the synthetic oxide.

Physicochemical parameters	Values
Nature	Crystalline
Titanium content (%)	53.4 (±0.2)
Thermal water loss (%)	20.6 (±0.2)
Bulk density (g cm^{-3})	1.21 (±0.05)
Dimension (nm) of particle (TEM)	11–13
Specific surface area (m^2 g^{-1})	663 (±5.5)
pH_{zpc}	6.5 (±0.3)

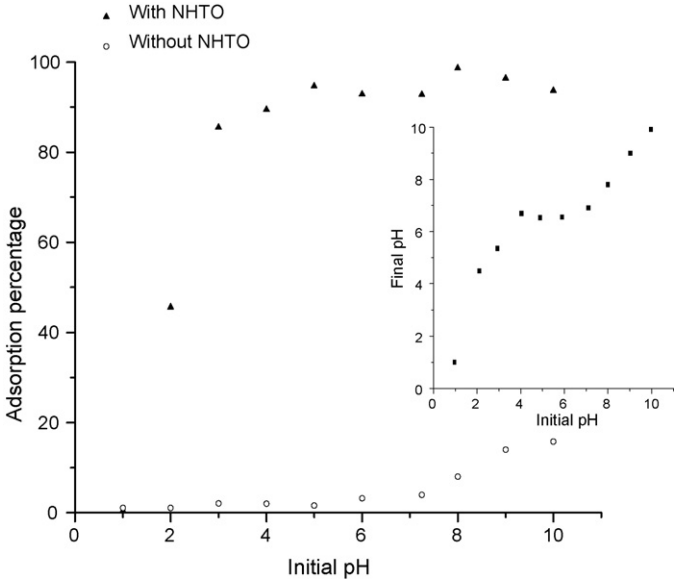

Fig. 6. The plot of initial solution pH (pH_i) vs. percentage adsorption of Ni(II) from the aqueous solution ($C_0 = 10.0\ mg\ L^{-1}$) by NHTO at 30 °C.

3.2. Effect of pH

Fig. 6 demonstrates the variation of adsorption percentage of Ni(II) against pH_i from the aqueous solution ($C_0 = 10.0\ mg\ L^{-1}$) in the presence and absence of NHTO. It was found that the adsorption percentages of Ni(II) enhanced with increasing pH_i from 1.0 to 5.0 and, remained nearly constant up to pH_i 10.0. The disappearance of Ni(II) from solution in the absence of NHTO at $pH_i \geq 6.0$ is presumed to be for the precipitation of metal ion as hydroxide. Thus, the removal of Ni(II) at $pH_i \geq 6.0$ is due to the combined effect of (i) precipitation as $Ni(OH)_2$ and (ii) adsorption on the surface of NHTO. Thus, the optimum pH_i for the removal of Ni(II) by adsorption was fixed up at 5.0 (±0.1) for the next steps of experiments, which has been found to be similar to that used by Hasar [26] on adsorption of Ni(II) from aqueous solution onto activated carbon.

The change of equilibrium solution pH (pH_f) from pH_i was also noted and demonstrated (inset of Fig. 6). The pH_f was found to be higher than pH_i ranged in 1.0–6.0, and that was lower than pH_i ranged in 7.0–10.0. The pH_{zpc} of NHTO was ranged between 6.0 and 7.0. The mechanism of Ni(II) adsorption can thus be described as

$$TiO_2{\cdot}(OH^-)_x + H^+ + 0.5Ni^{2+} \rightarrow 0.5Ni^{2+}\text{---}^{-}OH{\cdot}TiO_2(OH^-)_{x-2} + H_2O$$

$$(\text{at } pH_i < pH_{zpc})$$

$$2[TiO_2(OH^-)_x] + 2OH^- + 0.5Ni^{2+} + NiOH^+ \rightarrow 0.5Ni^{2+}\text{---}^{-}OH{\cdot}TiO_2(OH^-)_x + NiOH^+\text{---}^{-}HO{\cdot}TiO_2(OH^-)_x$$

$$(\text{at } pH_i > pH_{zpc})$$

The NHTO surface was negative (confirmed from the mobilization in electrical field) as the material used for adsorption reaction was precipitated at pH 7.5 ± 0.1. Thus, the variation of pH_f from pH_i described the reaction mechanism.

3.3. Effect of initial concentration (C_0) and temperature (T) on Ni(II) adsorption reaction

The effects of C_0 (=10.0, 30.0 and 50.0 mg L^{-1}) and T (=15°, 30°, 45° and 55 °C) on the adsorption reaction of Ni(II) with NHTO at pH_i 5.0 (±0.1) were investigated. Fig. 7 demonstrates the results. It was

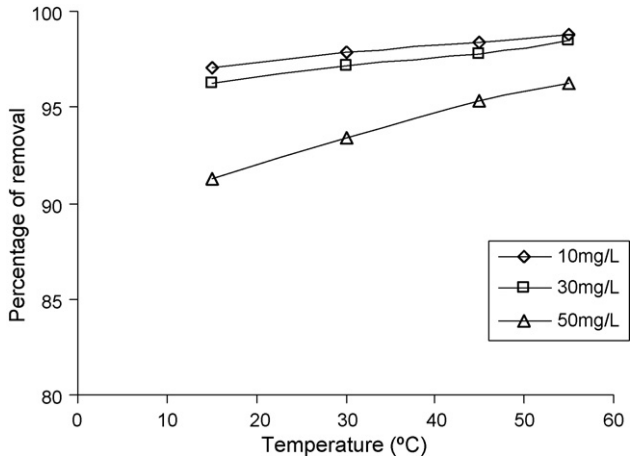

Fig. 7. The effect of temperature and concentration on Ni(II) adsorption by NHTO.

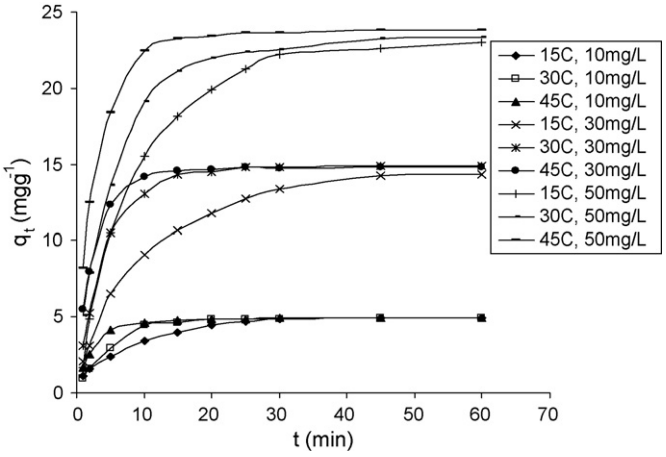

Fig. 8. The plot of Ni(II) adsorption capacity (q_t, mg g^{-1}) vs. contact time (t, min) at different temperatures and pH$_i$ 5.0 (±0.1).

found that that the differences of removal percentage of Ni(II) were found to be small for the metal ion solution of C_0 between 10.0 and 30.0 mg L^{-1} at any reaction temperature. The removal percentage of Ni(II) increased from 95.0 (±1.0) to 98.0 (±1.0) when C_0 increased from 10.0 to 30.0 mg L^{-1}, while that was 91.0 (±1.0) to 96.0 (±1.0) for C_0 = 50.0 mg L^{-1} with increasing T from 15 to 55 °C. In general, the removal percentage increased with rising T on the reaction. The increase of Ni(II) removal percentage with rising T indicated that the reaction of Ni(II) adsorption with NHTO was endothermic. This is the general feature of the endothermic reaction as per Le-Chatelier principle of equilibrium reaction.

3.4. Kinetic analysis

Fig. 8 demonstrates the variation of q_t (mg g^{-1}) with increasing reaction time, t (min) at pH$_i$ 5.0 (±0.1) by NHTO at T = 15, 30 and 45 °C. It was found that ~94.0 (±1.0)% of q_e (mg g^{-1}) of Ni(II) took place at a t ~20 min of the reaction, and the time required in reaching plateau of q_t was 30 min giving q_e for the reaction at T = 30 and 45 °C while that was 40 min when T is 15 °C. The time (in minute) required in reaching equilibrium (t_e) was found to be much less than that reported with kaolinite and montmorillonite [31,32]. The q_t-values of Fig. 8, taking up to the point of t_e assuming the data beyond t_e will have no/little influence on the reaction rate, were analyzed using Eqs. (2)–(4) by the non-linear method of analysis on the origin software spread sheet.

Pseudo-first order [47]:

$$q_t = q_e\{1 - \exp(-k_1 t)\} \quad (2)$$

Pseudo-second order [48]:

$$q_t = \left\{ \frac{t}{1/k_2 q_e^2} + \left(\frac{t}{q_e}\right) \right\} \quad (3)$$

Elovich [49]:

$$q_t = \left(\frac{1}{\beta}\right) \ln(\alpha\beta) + \left(\frac{1}{\beta}\right) \ln(t) \quad (4)$$

where k_1 (min^{-1}) and k_2 (mg g^{-1} min^{-1}) are the pseudo-first order and pseudo-second order rate constants, respectively; the q_t and q_e have the significance mentioned elsewhere; α and β are the Elovich constants of Eq. (4).

Table 2
The kinetic parameters of Ni(II) adsorption on NHTO at pH$_i$ 5.0 (±0.1) at different temperatures and concentrations.

Model	Parameters	10 mg L^{-1}			30 mg L^{-1}			50 mg L^{-1}		
		15 °C	30 °C	45 °C	15 °C	30 °C	45 °C	15 °C	30 °C	45 °C
Pseudo-first order	k_1 (min^{-1}) (×10^{-1})	1.46	1.98	3.81	1.15	2.31	4.02	1.13	1.93	3.63
	q_e (mg g^{-1})	4.64	4.92	5.05	13.48	14.79	15.15	22.03	22.75	23.47
	R^2	0.99	1.00	1.00	1.00	1.00	0.99	1.00	0.99	0.99
	χ^2 (×10^{-2})	0.02	0.91	0.72	0.58	41.95	8.12	21.27	33.65	41.18
Pseudo-second order	k_2 (mg L^{-1} min^{-1}) (×10^{-2})	0.28	0.43	0.78	5.42	13.56	22.78	25.55	42.36	84.95
	q_e (mg g^{-1})	5.35	5.56	5.76	16.02	16.56	16.78	25.10	25.76	26.10
	R^2	0.98	0.97	0.98	0.99	0.98	0.98	0.99	0.99	0.99
	χ^2 (×10^{-2})	3.87	7.17	3.06	2.26	47.94	23.65	58.33	39.76	42.16
Elovich	α	2.45	3.35	13.35	4.89	12.45	49.27	7.84	16.20	59.15
	B (×10^{-2})	95.35	92.99	125.47	30.11	32.30	43.23	17.54	20.39	25.59
	R^2	0.95	0.91	0.86	0.79	0.90	0.86	0.96	0.95	0.88
	χ^2 (×10^{-2})	1.21	23.48	21.24	67.28	207.68	184.62	133.61	265.94	413.73
Intra-particle	k_{id1} (mg g^{-1} min$^{-0.5}$)	1.02	1.32	1.81	2.73	4.12	4.95	4.44	5.72	7.67
	k_{id2} (mg g^{-1} min$^{-0.5}$) (×10^{-2})	2.04	5.92	5.15	27.3	13.34	5.69	35.62	41.52	14.38
	C (mg g^{-1})	4.48	4.50	4.58	11.47	13.95	14.40	20.24	20.26	22.80
	R^2_1	0.99	0.96	0.99	0.97	0.95	0.89	0.96	0.98	0.94
	R^2_2	0.97	0.50	0.69	0.91	0.67	0.71	1.00	0.94	0.85
	SSE	2.65	6.05	3.50	18.99	55.56	29.74	81.07	93.59	97.10
Pore diffusion	D_p (cm^2 s^{-1}) (×10^{-8})	0.62	0.87	11.73	0.58	1.10	1.28	0.59	0.71	1.92
Film diffusion	D_F (cm^2 s^{-1}) (×10^{-7})	2.26	3.03	6.10	1.97	3.89	4.52	1.96	2.35	6.54

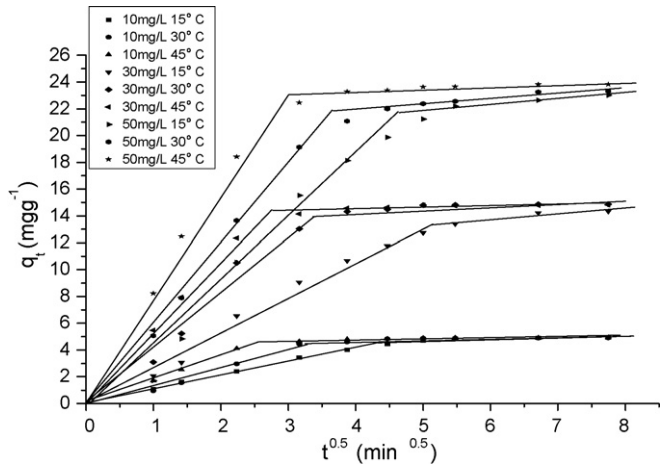

Fig. 9. The Weber–Morris plot of the kinetic data for Ni(II) adsorption by NHTO from aqueous solution at pH_i 5.0 (±0.1).

Table 2 shows the estimated kinetic parameters. Based on the values of statistical error χ^2 (chi square) and the linear regression coefficient (R^2), it could be suggested that the present q_t-values described the pseudo-first order Eq. (2) well (R^2 = 0.99–1.00), and better than the pseudo-second order Eq. (3) (R^2 = 0.97–0.99). However, the difference of goodness of data fit between the pseudo-first order and the pseudo-second order equations was small. Besides these, the q_t of Fig. 8 described the Elovich Eq. (4) poorly (R^2 = 0.79–0.96). Thus, the order of data fit, in general, is pseudo-first order > pseudo-second order > Elovich equation. The q_e had increased with increasing C_0 at a particular T on the reaction. However, the increase of q_e was found to be less with increasing T on the reaction at any particular C_0 of the solute. Thus, it can be concluded that the T has small positive influence on the present adsorption reaction. The rate constant (k_1 or k_2) values had increased with increasing T on the reaction at any particular C_0 of Ni(II). The observed dependence of rate constant on the C_0 and T has indicated that the Ni(II) adsorption performance for removal by NHTO is increasingly well with lowering of C_0 and increase of T on the reaction.

3.5. Diffusion kinetics

The overall solute adsorption onto the solid surface may be controlled by one or more steps, e.g., boundary layer (film) or external diffusion, pore diffusion, surface diffusion and adsorption onto the pore surface or in combination of several steps. Generally, an adsorption process is diffusion controlled if the rate is dependent upon the rate of diffusion of the components towards one another. According to Weber and Morris [50], if the rate-limiting step (RLS) is intra-particle diffusion, then the value of q_t shown in Fig. 8 as a function of t should be directly proportional to the square root of contact time t, which is defined mathematically as (Eq. (5)),

$$q_t = k_{id} t^{0.5} + C \tag{5}$$

where C (mg g^{-1}) is the boundary layer thickness and k_{id} (mg g^{-1} min$^{-1/2}$), the intra-particle diffusion rate constant. Greater is the value of C greater is the effect of the boundary layer on the adsorption process. The plot of q_t with respect to $t^{0.5}$ will yield a straight line with intercept equal to C. If the Weber–Morris plot of q_t versus $t^{0.5}$ gives a single straight line with C = 0, the sorption rate should be controlled by intra-particle diffusion only. But, if the plot of the data produces multi-linear portions, then two or more steps influence the sorption process.

Fig. 9 demonstrates the plots q_t versus $t^{0.5}$. It was found that two straight lines relate the points—the sharp first linear portion is due to the boundary layer (film) diffusion and the second linear one is for the pore diffusion [51]. The non-linearity of plots over a range of $t^{0.5}$ had indicated the multistage adsorption of Ni(II) by NHTO. Extrapolation of the linear portions of the plots back to the y-axis gave the intercept, providing the measure of the boundary layer thickness (C). The deviation of the straight line from the origin might be due to the difference in rate of mass transfer at t = 0 and $t = t_e$ stages of adsorption. Further, the deviation of straight line from the origin indicated that the RLS was not pore diffusion. The initial curvature in the plots has attributed to the boundary layer effect or external mass transfer effect. The slope of the first portion of the plot has indicated the boundary layer (film) diffusion characteristics of the adsorption while that of the second linear portion is for the pore diffusion. The values for k_{id1} and k_{id2} were computed from the slope of each plot. Table 2 shows the values of these parameters (k_{id1}, k_{id2} and C). The values of k_{id1} were about hundred times greater than that of k_{id2}, and suggested that the boundary layer (film) diffusion had controlled the present adsorption process. As the present reaction was very fast and the t_e values were 30 min at 30 and 45 °C and 45 min at 15 °C, the reaction obviously depends upon the active sites on outer surface of solid indicating the first order kinetics and boundary-layer (film) diffusion model. In order to confirm the above, the intra-particle diffusion (pore) coefficients (D_p, cm^2 s^{-1}) were calculated by Eq. (6) [51,52]:

$$D_p = \frac{0.03\, r_0^2}{t_{0.5}} \tag{6}$$

where 'r_0' (cm) is the average radius of the adsorbent particle, and $t_{0.5}$ (min), the time required to complete the half of the adsorption. According to Michelsen et al. [52], if the calculated values of D_p be ranged in 10^{-11} to 10^{-13} cm^2 s^{-1}, the RLS will be the intra-particle diffusion and, if the calculated film diffusion co-efficient (D_F, cm^2 s^{-1}) value be ranged in 10^{-6} to 10^{-8}, then the RLS will be controlled by the boundary-layer (film) diffusion. But in this study, the calculated values of D_p were in no cases the order of 10^{-11} cm^2 s^{-1}. The calculated values of D_p were in the order of 10^{-8} cm^2 s^{-1} (Table 2), and at least thousand times more than the 10^{-11} cm^2 s^{-1}. This had indicated that the RLS for the Ni(II) adsorption by NHTO is not the intra-particle diffusion. The values of D_F were also calculated by Eq. (7) [52,53]:

$$D_F = \frac{0.23\, r_0 \delta C_s}{C_L t_{0.5}} \tag{7}$$

where r_0 and $t_{0.5}$ have the same meaning as above, δ the film thickness (10^{-3} cm) [53], C_s and C_L are the concentrations (mg g^{-1}) of adsorbate in solid and liquid phases at $t = t$ and t = 0, respectively. The values of D_F calculated were found in the order of 10^{-7} cm^2 s^{-1} (Table 2), which is in between 10^{-6} and 10^{-8} cm^2 s^{-1}. This had implied that the Ni(II) adsorption reaction with NHTO is a film (boundary-layer) diffusion phenomenon.

3.6. Determination of diffusivity

The Boyd kinetic model [53,54] has been used to analyze the data of Fig. 8, which is valid under the conditions of experiments. With diffusion rate controlling in the adsorption on particles of spherical shape, the solution of the simultaneous set of differential and algebraic equation lead to Eq. (8).

$$F(t) = 1 - \frac{6}{\pi^2} \sum_{z=1}^{\infty} \frac{1}{z^2} \exp\left[\frac{-z^2 \pi^2 D_e t}{R_a^2}\right] \tag{8}$$

where $F(t) = q_t/q_e$ is the fractional attainment of equilibrium at time t, D_e the effective diffusion coefficient of adsorbate in the adsorbent

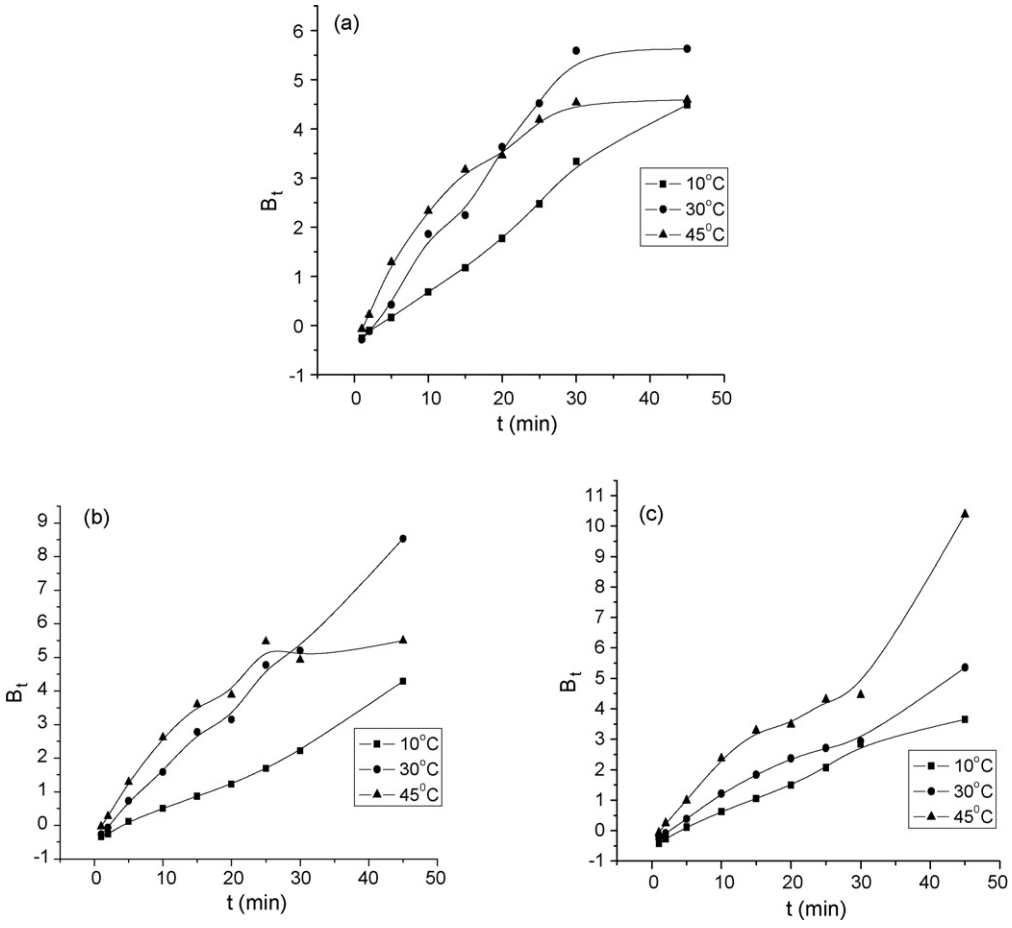

Fig. 10. The Boyd Kinetic plots for the Ni(II) adsorption with variation of temperature and concentration (C_0, mg L^{-1}) (a) 10.0, (b) 30.0, and (c) 50.0.

phase ($cm^2\ s^{-1}$), R_a the radius of the adsorbent particles assumed to be spherical (cm) and z is an integer. Eq. (8) on simplification attains the form (9)

$$F = 1 - \frac{6}{\pi^2}\ \exp(-B_t) \tag{9}$$

B_t is simplified as Eq. (10)

$$B_t = -0.4985 - \ln\left[1 - \left(\frac{q_t}{q_e}\right)\right]. \tag{10}$$

Taking the determined q_t and q_e values, the B_t were calculated using Eq. (10) and plotted against t. Fig. 10 shows non-linearity over the range of adsorption time, which had indicated that the adsorption reaction is not controlled by the intra-particle diffusion. This supported the result that had been described earlier. The results obtained had been found to be similar with those reported on adsorption of (i) chromium on crystalline hydrated titanium oxide [10] and (ii) dye on unburned carbon [55].

3.7. Isotherm modeling

Fig. 11 demonstrates the equilibrium data as points obtained on the adsorption of Ni(II) by NHTO at temperatures T (±1 °C) = 15 °C (a), 30 °C (b), 45 °C (c) and 55 °C (d). To evaluate the nature of the adsorption reaction, the data shown in Fig. 11 were analyzed with the non-linear fit method on the origin-spread sheet of computer using Eqs. (11)–(13) [56]:

$$\text{Langmuir model}: \ q_e = \frac{q_m K_a C_e}{1 + K_a C_e} \tag{11}$$

$$\text{Freundlich model}: \ q_e = K_F C_e^{(1/n)} \tag{12}$$

$$\text{Redlich–Peterson model}: \ q_e = \frac{AC_e}{1 + BC_e^g} \tag{13}$$

where q_e has usual significance and given elsewhere, q_m the monolayer adsorption capacity (mg g^{-1}), C_e is the equilibrium solute concentration (mg L^{-1}), K_a (L mg^{-1}), K_F (mg g^{-1}), n, A and B are the Langmuir, Freundlich and Redlich–Peterson (R–P) isotherm constants, respectively. Fig. 11 demonstrates the non-linear line fits of the adsorption data of Ni(II) on NHTO. Table 3 shows the estimated parameters related with isotherm Eqs. (11)–(13) including statistical error chi-square (χ^2) and standard square error (SSE). Based on the regression coefficient (R^2), standard square error (SSE) and the statistical error chi-square (χ^2) values, it was concluded that the experimental data fits were best with the three-parameter R–P isotherm Eq. (13) ($0.97 \le R^2 \le 0.99$, SSE = 2.10–10.74, and χ^2 = 0.30–1.53) and, the goodness of data fits was fairly well with the models, viz., the Langmuir Eq. (11) (R^2 = 0.96; SSE = 16.57, 21.34 and χ^2 = 2.07, 2.67) at 45 and 55 °C, and the Freundlich Eq. (12) (R^2 = 0.96, 0.97; SSE = 10.74, 11.97 and χ^2 = 1.34, 1.50) at 15 and 30 °C, respectively. The goodness of data fit with the R–P Eq. (13) was closer to the Langmuir Eq. (11) than the Freundlich Eq. (12) at two higher temperatures (T = 45 and 55 °C), while that was slightly nearer to the Freundlich than that of the Langmuir at two lower temperatures (T = 15 and 30 °C). The R–P model Eq. (13) converts to (i) the Langmuir type (Eq. (11)) when g = 1.0 and (ii) the Freundlich type (Eq. (12)) when g = 0. The values for g of the R–P model Eq. (13) had increased from 0.82 to 0.93 with increasing T from 15 to 55 °C, respectively. The values of g (Table 3) of the R–P model

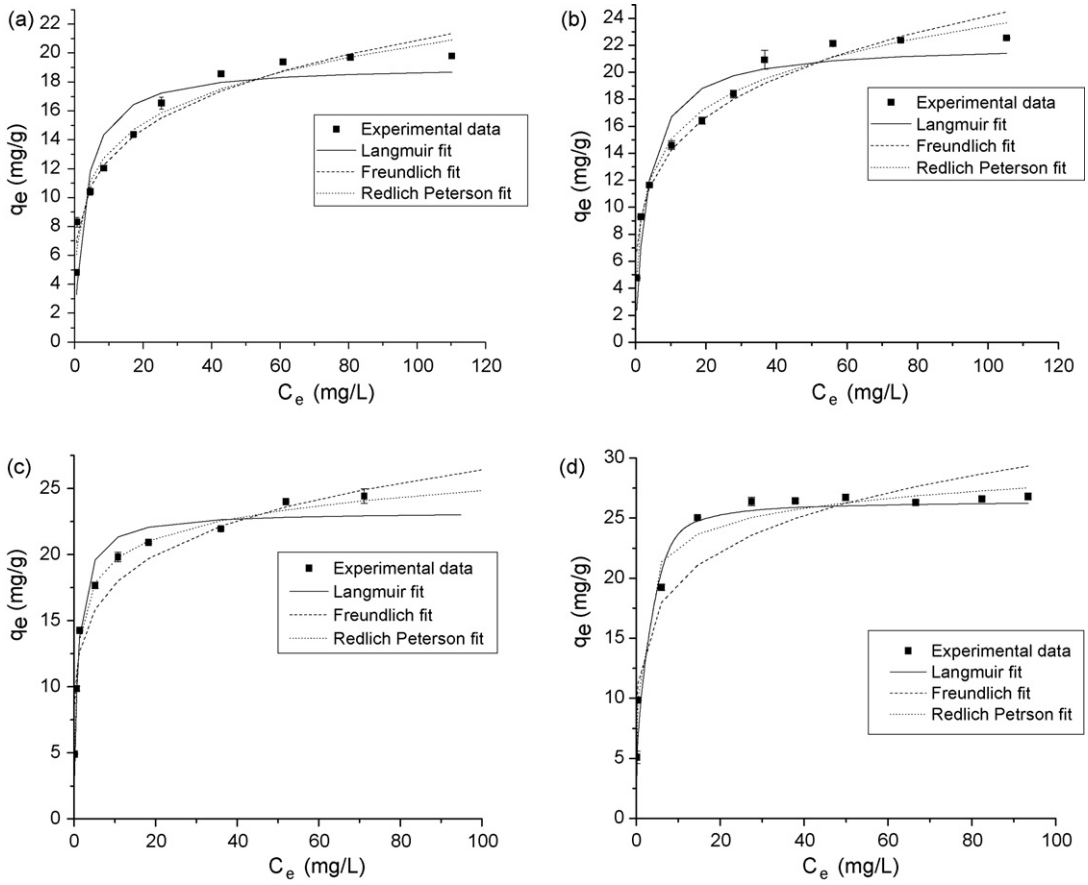

Fig. 11. The equilibrium data (points) on Ni(II) adsorption from aqueous solution at pH_i 5.0 (±0.1) by NHTO at (a) 15 °C, (b) 30 °C, (c) 45 °C, and (d) 55 °C with non-linear fits of isotherm model equations.

isotherm had suggested the presence of slight less Langmuir characteristics at T = 15 and 30 °C than at T = 45 and 55 °C on the Ni(II) adsorption reaction with NHTO. Thus, this has indicated that the surface sites of heterogeneous type transforms to more homogeneous with increasing T from 15 to 55 °C, and the reaction becomes increasingly monolayer type with rising T on the reaction. To access the performance of Ni(II) adsorption by NHTO, the q_m (mg g^{-1}) had been compared with some reported data (Table 4) [26,28,57–67]. It has been seen that the Ni(II) removal efficiency of the present material is either better or comparable with many other adsorbents investigated.

Table 3
Analyzed isotherm parameters on Ni(II) adsorption by NHTO at pH_i 5.0 (±0.1) at different temperatures.

Isotherm equations	Parameters	Temperature (±1 °C)			
		15°	30°	45°	55°
Langmuir	K_a (L mg^{-1}) (×10^{-2})	34.68	30.47	103.61	119.08
	q_m (mg g^{-1})	19.18	22.07	23.24	26.47
	R^2	0.85	0.92	0.96	0.96
	SSE	37.23	27.76	16.57	21.34
	χ^2	4.65	3.47	2.07	2.67
Freundlich	K_f (mg g^{-1})	7.69	8.34	11.93	13.06
	n	4.60	4.32	5.79	5.61
	R^2	0.96	0.97	0.92	0.90
	SSE	10.74	11.97	31.09	57.26
	χ^2	1.34	1.50	3.89	7.16
Redlich–Peterson	A (L g^{-1})	34.84	24.81	43.97	47.24
	B (L mg^{-1})	4.32	2.30	2.61	2.30
	g	0.82	0.83	0.91	0.93
	R^2	0.97	0.98	0.99	0.98
	SSE	8.64	5.33	2.10	10.74
	χ^2	1.23	0.76	0.30	1.53

3.8. Adsorbate coverage

Comparisons of adsorption characteristics for adsorbent of various surface areas or void structures on various adsorbates by surface coverage are helpful in understanding the interaction between adsorbates and the surfaces of adsorbents, thus facilitates the designing and preparing of adsorbents which meets the particular need.

Taking the monolayer coverage of Ni(II) on the surface of NHTO particle, and the covered mass (q_m) of 30 °C (estimated from the Langmuir equation), the projected area of adsorbate molecule (A_m, m^2) (here, hydrated Ni(II) ion), the adsorbate coverage per unit gram of NHTO (S_c, m^2 g^{-1}) could be calculated using Eq. (14) [68]:

$$S_c = \frac{6.023 \times 10^{23} \times A_m \times q_m}{1000}. \quad (14)$$

The value of S_c obtained was 812.83 m^2 g^{-1}. This indicated that the Ni(II) ions were very well attracted by the NHTO surface and the specific surface area increased due to Ni(II) adsorption from 663 (±5.5) to 812.83 m^2 g^{-1}. The increase of surface area has indicated that the NHTO can be used as an adsorbent for scavenging the Ni(II) ion from aqueous solution.

3.9. Effect of diverse ions during adsorption

The ions (with concentration range used), which are found commonly in waste/ground water, had been used to investigate the

Table 4
Comparison of Langmuir capacity (q_m) with some reported data on Ni(II) adsorption by adsorbents from aqueous solution.

Adsorbent	pH	C_0 (mg L^{-1})	q_m (mg g^{-1})	Ref.
Modified activated carbon from almond husk	5.0	25.0–250.0	37.175	[26]
Tea waste	4.0	50.0–300.0	15.26	[28]
Oil palm ash	5.0	472.1–629.5 μmol L^{-1}	168.8 μmol g^{-1}	[57]
Powdered egg shell	–	–	0.007	[58]
Ecklonia Biomass	4.0	50.0–500.0	23.4	[59]
Grape stalks waste	6.0	2.4×10^{-4} to 2.4×10^{-3} mol L^{-1}	1.82×10^{-4} mol g^{-1}	[60]
Dye loaded jute fibre	6.58	82.3–456.6	5.26	[61]
Oxidised jute fibre	6.58	82.3–456.6	5.57	[61]
Unmodified jute fibre	6.58	82.3–456.6	3.37	[61]
Montmorillonite	6.5–7.0	10.0–250.0	28.4	[62]
Acid-activated montmorillonite:	6.5–7.0	10.0–250.0	29.5	[62]
Bagasse fly ash (BFA)	6.0	50.0–500.0 mmol L^{-1}	0.4316 mmol g^{-1}	[63]
Rice husk ash (RHA)	6.0	50.0–500.0 mmol L^{-1}	0.2839 mmol g^{-1}	[63]
Sphagnum moss peat	5.0	25.0–300.0	8.52	[64]
Solid humic acid	3.7	4.0–100.0	0.469 mmol g^{-1}	[65]
Water insoluble magnetic calcium-alginate microcapsules	5.3 ± 0.13	2.0–150.0 mmol L^{-1}	0.52 mmol g^{-1}	[66]
Natural iron-oxide coated sand	7.0	30.0–90.0	1.26	[67]
NHTO	5.0 ± 0.1	10.0–150.0	22.07	Present work

Table 5
The adverse effect of some ions on the removal of Ni(II) by NHTO at pH_i 5.0 (± 0.1) and 30 °C.

Competing ion (C.I)	Mole ratio C.I:Ni(II)	Percentage of adsorption	Competing ion (C.I)	Mole ratio C.I:Ni(II)	Percentage of adsorption
Cl^-	5.01	93.26	Fe(III)	0.03	45.82
	10.02	91.26		0.16	34.14
	15.03	89.69		0.32	25.23
	20.04	88.23		0.63	15.42
SO_4^{-2}	0.46	91.65	Ca(II)	0.73	92.25
	0.93	89.26		1.47	90.23
	1.85	87.23		2.20	88.23
	3.70	84.35		2.93	87.36
Cr(VI)	0.31	91.56	Mg(II)	1.22	92.91
	0.62	89.56		2.44	89.27
	0.94	88.56		3.67	88.81
	1.25	87.14		4.89	87.56
Removal percentage of Ni(II)in the absence of any competing ion					95.27

adverse influence, if any, on the adsorption reaction of Ni(II) with NHTO. The results (Table 5) show that the removal percentages of Ni(II) by NHTO were ranged in 84.0–93.0 compared to that obtained (95.0%) in the absence of any diverse ion. This had indicated that the Ni(II) removal by NHTO reduced slightly in the presence of the used diverse ions, excepting Fe(III). The chloride which has commonly found to be present at high concentration in water showed insignificant adverse effect on Ni(II) adsorption. The percentage of removal was ~95.0 in the presence of zero Cl^-:Ni(II) mole ratio, and that reduced to 88.0 when the mole ratio enhanced from 5.01 to 20.04. The removal percentages were also found to be ≥84.0 to ≤93.0 in the presence of other ions (Table 4). However, the substantial reduction in the removal percentage of Ni(II) was found in the presence of Fe(III). It was found that the percentage of removal reduced from ~95.0 to ~46.0 with increasing Fe(III):Ni(II) mole ratio from 0 to 0.03, and that became ~15.0 when the mole ratio enhanced to 0.63. This has indicated that the Fe(III) competes strongly with Ni(II) for the binding sites on NHTO surfaces for adsorption at the conditions of experiment. It might be due to the higher positive charge on Fe(III) and chemical closeness with Ni(II).

3.10. Evaluation of adsorption energy

The equilibrium data shown (as points) in Fig. 11 were analyzed by Dubinin–Radushkevick (D–R) Eq. (15) [69,70] for evaluating the adsorption energy.

$$\ln q_e = \ln q'_m - K_{DR}\varepsilon^2, \quad (15)$$

$$\varepsilon = RT \ln\left(1 + \frac{1}{C_e}\right) \quad (16)$$

where ε is the Polanyi potential, q'_m the D–R adsorption capacity (mol kg^{-1}), and K_{DR} is a constant related to adsorption energy (mol^2 kJ^{-2}). The q'_m and K_{DR} parameters were evaluated from the intercepts and slopes of the plots of $\ln q_e$ versus ε^2 (plots omitted). The mean free energy of adsorption (E_{DR}) is the free energy change when 1 mol of ion is transferred to the surface of the adsorbent from infinity in the solution [69,70] and, it was calculated using Eq. (17):

$$E_{DR} = (-2K_{DR})^{-1/2} \quad (17)$$

Table 6 demonstrates the estimated parameters of the D–R equation with E_{DR}. The magnitude of E_{DR} is useful for estimating the type of adsorption reaction and, if it be ranged in 8.0–16.0 kJ mol^{-1}, the adsorption reaction should be taken place by electrostatic mechanism [69,70]. The E_{DR} values obtained for the present case were ranged between 8.0 and 16.0 kJ mol^{-1} for 15 and 30 °C, and that were very close to 16 kJ mol^{-1} for the 45 and 55 °C. The E_{DR} val-

Table 6
The Dubinin–Radushkevick (D–R) isotherm equation parameters on Ni(II) adsorption by NHTO at pH_i 5.0 (±0.1).

T (±1.6 K)	K_{DR} (mol^2 kJ^{-2}) (×10^{-9})	q'_m (mol kg^{-1}) (×10^{-4})	E_{DR} (kJ mol^{-1})	R^2
288	2.85	7.31	13.25	1.00
303	2.51	8.08	14.11	0.99
318	1.92	9.21	16.14	0.98
328	1.87	10.25	16.35	0.98

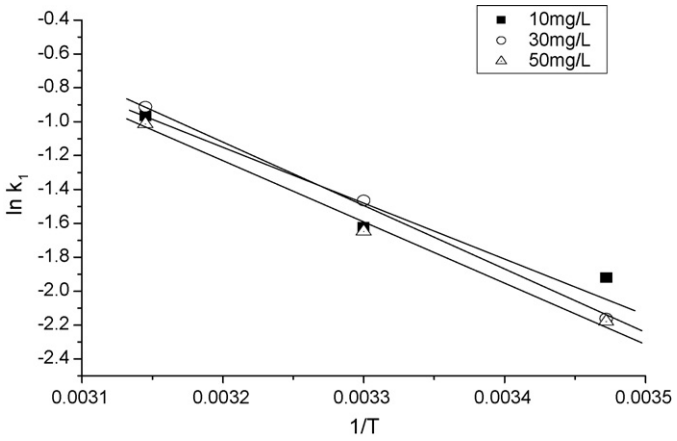

Fig. 12. The plot of $\ln k_1$ vs. $1/T\,(K^{-1})$ for the activation parameters with variation of Ni(II) concentration in solution.

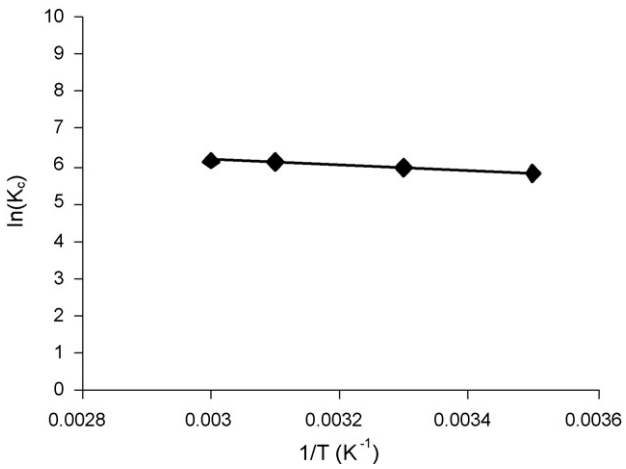

Fig. 13. The Vant Hoff's plot for thermodynamic parameters.

ues thus indicated that the Ni(II) adsorption on NHTO had taken place mainly by electrostatic mechanism with some other inherent mechanisms lying within for the reactions especially at higher two temperatures.

3.11. Activation parameters

The relation between the rates constant (k_1) with reaction temperature may be described by the Arrhenius Eq. (18):

$$k_1 = A \exp\left(-\frac{E_a}{RT}\right) \tag{18}$$

The rate constant, k_1 is considered here as the pseudo-first order rate constant (min^{-1}). A is a temperature independent factor ($g\,mg^{-1}\,min^{-1}$), E_a the activation energy of adsorption ($kJ\,mol^{-1}$), R the molar gas constant ($8.314\,J\,mol^{-1}\,K^{-1}$) and T the absolute temperature (K). Taking logarithmic of Eq. (18), the following Arrhenius type linear Eq. (19) is obtained.

$$\ln k_1 = \ln A + \left(-\frac{E_a}{R}\right)\frac{1}{T} \tag{19}$$

The plot of $\ln k_1$ against $1/T$ shows a linear (Fig. 12) variation with high value of regression coefficient ($R^2 = 0.95$–1.00).

The intercept and slope of the plots gave the temperature independent parameter, A (3.33×10^3, 6.81×10^4 and $2.54 \times 10^4\,g\,mg^{-1}\,s^{-1}$) and the activation energy, E_a (24.13, 31.79 and 29.57 $kJ\,mol^{-1}$), respectively. The results obtained had been found to be similar to that had been reported by Daifullah et al. [71] and Ozcan et al. [72].

3.12. Thermodynamic parameters

The thermodynamic parameters such as change in Gibbs free energy (ΔG°, $kJ\,mol^{-1}$), enthalpy (ΔH°, $kJ\,mol^{-1}$), and entropy (ΔS°, $kJ\,mol^{-1}\,K^{-1}$) of the adsorption reaction are used to determine spontaneity of the process and whether it is endothermic or exothermic. The ΔG° is related to the equilibrium constant, ($K_c = q_e/C_e$) by the following Eq. (20):

$$\Delta G^\circ = -RT \ln K_c \tag{20}$$

The terms present have their usual significance and given elsewhere.

According to thermodynamics, the ΔG° is also related to ΔH° and ΔS° at constant temperature by the following Eq. (21):

$$\ln K_c = \left(\frac{\Delta S^\circ}{R}\right) - \left(\frac{\Delta H^\circ}{RT}\right) \tag{21}$$

The values of ΔH° and ΔS° were calculated from the slope and intercept of the linear plots ($R^2 = 0.98$) of $\ln K_c$ versus T^{-1} (Fig. 13). Table 7 shows the estimated values of thermodynamic parameters. It was found that the $-\Delta G^\circ$ values increased with increasing T and indicated the enhancement of feasibility and spontaneity of Ni(II) adsorption reaction with NHTO. The positive ΔH° value (Table 6) suggested the endothermic nature of the reaction, which is opposite to that reported by Bhattacharyya and Sen Gupta [31,32]. The positive ΔS° value (Table 6) indicated also that this reaction took place with the increase in number of species at the solid–liquid interface and, hence the randomness at the (solid + liquid) interface. This is presumably due to the release of aqua molecules at interface when the aquated Ni(II) is adsorbed on the surface of the adsorbent. The low positive value of ΔH° (much less than $40\,kJ\,mol^{-1}$) indicates the physisorption of Ni(II) on NHTO.

3.13. Confirmation of the favorability of the adsorption process

To confirm the favorability of the Ni(II) adsorption by NHTO, the separation factor (R_L) was calculated using the following Eq. (22) [33,48,49]:

$$R_L = \frac{1}{1 + K_a C_0} \tag{22}$$

where R_L is a dimensionless separation factor indicating the shape of the isotherm, K_a and C_0 have their usual significance as specified earlier. The isotherm is (i) unfavorable when $R_L > 1$, (ii) linear when $R_L = 1$, (iii) favorable when $R_L < 1$ and (iv) irreversible when $R_L = 0$. The values of R_L were calculated by taking K_a, obtained from the non-linear analysis of Langmuir isotherm and the lowest C_0 ($10.0\,mg\,L^{-1}$) that used for the equilibrium isotherm studies were found to be 0.224, 0.247, 0.088 and 0.078 at $T = 15$, 30, 45 and 55 °C, respectively. The R_L values were laid above zero and much below 1.0 indicating the favorable adsorption of Ni(II) by NHTO, and that should be true for the other higher C_0 used for equilibrium studies. The R_L values, in general, had revealed that the NHTO is a good

Table 7
Thermodynamic parameters evaluated on Ni(II) adsorption by NHTO at pH_i 5.0 (±0.1).

Adsorbate species	Temperature (±1 °C)	$-\Delta G^\circ$ ($kJ\,mol^{-1}$)	$+\Delta H^\circ$ ($kJ\,mol^{-1}$)	$+\Delta S^\circ$ ($kJ\,mol^{-1}\,K^{-1}$)
Ni(II)	15	13.90	6.15	0.07
	30	15.05		
	45	16.22		
	55	16.30		

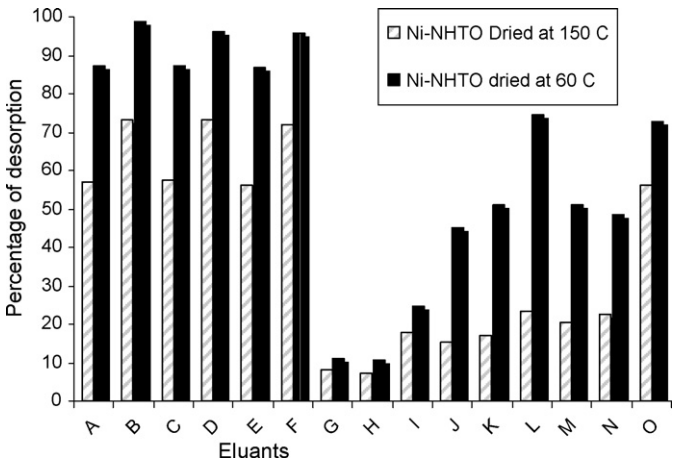

Fig. 14. Desorption of adsorbed Ni(II) from the Ni-NHTO using different eluants. A: 0.01 M HCl, B: 0.1 M HCl, C: 0.01 M HNO_3, D: 0.1 M HNO_3, E: 0.01 M H_2SO_4, F: 0.1 M H_2SO_4 G: 0.1 M NaCl, H: 0.1 M $NaNO_3$, I: 0.1 M Na_2SO_4, J: 1 M NaCl, K: 1 M $NaNO_3$, L: 1 M Na_2SO_4, M: 2 M NaCl, N: 2 M $NaNO_3$, and O: 2 M Na_2SO_4.

adsorbent for scavenging Ni(II) from the aqueous solution of any particular concentration.

3.14. Desorption study

The results on desorption of Ni(II) from the solid Ni-NHTO ($q_e = 26.90\,mg\,Ni\,g^{-1}$) by used different eluants at $30 \pm 1\,^{\circ}C$ are shown in Fig. 14. It was found that the percentages of Ni(II) released by 0.1 M HCl were ~98.0 and ~73.0, respectively, from the samples T-1 and T-2. The lower percentage of desorptions from the T-2 material than the T-1 had indicated stabilization of Ni(II) on NHTO surface with increasing drying temperature. Amongst the mineral acids used, HCl was found to be the most effective for this purpose. The percentage of Ni(II)-desorption from the sample T-1 with 0.1 M HCl was ~98.0 while that with 0.1 M HNO_3 and 0.1 M H_2SO_4, respectively, were ~ 96.0 and ~95.0. Again, the 0.1 M HCl was found to be slightly more efficient than the 0.01 M HCl to release the metal ion from the solid surfaces. This is due to the (a) greater H^+ concentration available from 0.1 M HCl than 0.01 M HCl, which compete well for the active sites where Ni(II) hosted on the solid and, (b) lower solution pH ($<pH_{zpc}$) converts the solid surface positive. The solutions of sodium salts of used corresponding acids were found to be much less efficient. The desorbed percentage from the Ni(II)-NHTO was ~75.0 by 1.0 M Na_2SO_4 which has been found much less compared to that of the acids tested, but higher than the other salt solutions used. The lower percentage of Ni(II) release by the salt solutions compared to the acids is due to the neutral solution pH. The higher percentage of release by Na_2SO_4 than the other used salts is presumably due to the available double Na^+ concentration in solution, which competes well for active sites where Ni(II) hosted on the solid. Thus, the best eluant found is 0.1 M HCl for the desorption of adsorbed Ni(II) from NHTO surfaces.

4. Conclusion

The synthetic titanium(IV) oxide (NHTO) was agglomerates of nanocrystallite particles of dimension 11–13 nm, hydrated and, the composite of brookite, anatase and rutile phases with irregular surface morphology. The specific surface area and pH_{pzc} of the synthetic oxide were 663.0 (±5.5) $m^2\,g^{-1}$ and 6.5 (±0.3), respectively. The optimum pH (pH_i) was 5.0 (±0.1) for the Ni(II) adsorption. The time required in reaching equilibrium was ~30 min indicating very fast reaction. The pseudo-first order rate equation described the adsorption kinetics very well. The film (boundary-layer) diffusion phenomenon influenced the adsorption rate. The Redlich–Peterson isotherm described the equilibrium data very well. The Fe(III) ion showed a strong negative influence on adsorption of Ni(II) by NHTO. The mean free energy of reaction indicated the columbic binding of the metal ion with the solid. The adsorption of Ni(II) by NHTO was spontaneous and endothermic and that took place with increasing entropy. The 0.1 M HCl desorbed 98% of adsorbed Ni(II) from the Ni-NHTO.

Acknowledgements

Authors are thankful to the Head, Department of Chemistry and the Principal, Presidency College for laboratory facilities. Authors are also grateful to Mr. Pulak Ray of Saha Institute of Nuclear Physics (Kolkata) for TEM analysis of the sample.

References

[1] A. Hagfeldt, M. Gratzel, Light induced redox reactions in nanocrystalline systems, Chem. Rev. 95 (1995) 49–68.
[2] S. Sakthivel, H. Kisch, Daylight photocatalyst by carbon modified titanium dioxide, Angew. Chem. Int. Ed. 42 (2003) 4908–4911.
[3] R.K. Sharma, M.C. Bhatnagar, G.L. Sharma, Mechanism in Nb doped titania oxygen gas sensor, Sens. Actuators B: Chem. 46 (1998) 194–201.
[4] K. Luchi, Y. Ohko, T. Tatsuma, A. Fujishima, Cathode separated TiO_2 photocatalyst applicable to photochromic device responsive to backside illumination, Chem. Mater. 16 (2004) 1165–1167.
[5] O. Carp, C.L. Huisman, A. Reller, Carbon-Inorganic hybrid materials: the carbon nanotube/TiO_2 interface, Solid Prog. State Chem. 32 (2004) 42.
[6] X.Z. Li, H. Liu, F. Cheng, H.J. Tong, Photocatalytic oxidation using a new catalyst-TiO_2 microsphere for water and wastewater, Environ. Sci. Technol. 37 (2003) 3989–3994.
[7] B.R. Manna, M. Dasgupta, U.C. Ghosh, Crystalline hydrous titanium(IV) oxide(CHTO): an arsenic (III) scavenger from natural water, J. Water SRT-Aqua 53 (2004) 483–495.
[8] S.C. Bhat, S. Goswami, S. Palchaudhury, U.C. Ghosh, Pb(II) sorption performance of hydrated titanium (IV) oxide from the aqueous solution, J. Ind. Chem. Soc. 82 (2005) 632–636.
[9] U.C. Ghosh, M. Dasgupta, S.C. Bhat, S. Debnath, Studies on management of chromium(VI)-contaminated industrial waste effluent using hydrous titanium oxide (HTO), Water Air Soil Pollut. 143 (2003) 245–256.
[10] S. Debnath, U.C. Ghosh, Kinetics, isotherm and thermodynamics for Cr(III) and Cr(VI) adsorption from aqueous solution by crystalline hydrous titanium oxide, J. Chem. Thermodyn. 40 (2008) 67–77.
[11] G.P. Rao, C. Lu, F. Su, Sorption of divalent metal ions from aqueous solution by carbon nanotubes: a review, Sep. Purif. Technol. 58 (2007) 224–231.
[12] K. Hristovski, A. Baumgardner, P. Westerhoff, Selecting metal oxide nanomaterials for arsenic removal in fixed bed columns: from nanopowders to aggregated nanoparticle media, J. Hazard. Mater. 147 (2007) 265–274.
[13] O. Friedrichs, T. Klassen, J.C. Sanchez-Lopez, R. Bormann, A. Fernandez, Hydrogen sorption improvement of nanocrystalline MgH_2 by Nb_2O_5 nanoparticles, Scripta Mater. 54 (2006) 1293–1297.
[14] M. Andersson, L. Osterlund, S. Ljungstrom, A. Palmqvist, Preparation of nanosize anatase and rutile TiO_2 by hydrothermal treatment of microemulsions and their activity for photocatalytic wet oxidation of phenol, J. Phys. Chem. B 106 (2002) 10674–10679.
[15] M. Kanna, S. Wongnawa, Mixed amorphous and nanocrystalline TiO_2 powders prepared by sol–gel method: characterization and photocatalytic study, Mater. Chem. Phys. 110 (2008) 166–175.
[16] A. Andrzejewska, A. Krysztafkiewicz, T. Jesionowski, Adsorption of organic dyes on the amino silane modified TiO_2 surface, Dyes Pigments 62 (2004) 121–130.
[17] L.C. Juang, C.K. Lee, C.C. Wang, S.H. Hung, M.D. Lyu, Adsorptive removal of acid red 1 from aqueous solution with surfactant modified titanate nanotubes, Environ. Eng. Sci. 25 (2008) 519–528.
[18] C.K. Lee, C.C. Wang, L.C. Juang, M.D. Lyu, S.H. Hung, S.S. Liu, Effects of sodium content on the microstructures and basic dye cation exchange of titanate nanotubes, Colloids Surf. A: Physicochem. Eng. Aspects 317 (2008) 164–173.
[19] C.K. Lee, K.S. Lin, C.F. Wu, M.D. Lyu, C.C. Lo, Effects of synthesis temperature on the microstructures and basic dyes adsorption of titanate nanotubes, J. Hazard. Mater. 150 (2008) 494–503.
[20] S.H. Sin, S.L. Lai, H.G. Leu, Removal of heavy metals from aqueous solution by chelating resin in a multistage desorption process, J. Hazard. Mater. B76 (2006) 139–153.
[21] A. Abu, F.A. Rub, M. Kandah, N.A. Dabaybeh, Nickel removal from aqueous solutions using sheep manure wastes, Eng. Life Sci. 2 (2002) 111–116.
[22] EPA U S, Guidance Manual for Electroplating and Metal Finishing Pretreatment Standards, 1984.
[23] K. Vijayaraghavan, J. Jegan, K. Palanivelu, M. Velan, Biosorption of cobalt(II) and nickel(II) by sea weeds: batch and column studies, Sep. Purif. Technol. 44 (2005) 53–59.

[24] K. Vijayaraghavan, J. Jegan, K. Palanivelu, M. Velan, Removal of nickel(II) ions from aqueous solution using crab shell particles in a packed bed up flow column, J. Hazard. Mater. B113 (2004) 223–230.
[25] Z. Aksu, D. Akpmar, Modeling of simultaneous biosorption phenol and nickel(II) onto dried aerobic activated sludge, Sep. Purif. Technol. 21 (2000) 87–99.
[26] H. Hasar, Adsorption of nickel(II) from aqueous solution onto activated carbon prepared from almond husk, J. Hazard. Mater. B97 (2003) 49–57.
[27] S. Al-Asheh, F. Banat, F. Mobai, Sorption of copper and nickel by spent animal bones, Chemosphere 39 (1999) 2087–2096.
[28] E. Malkoc, Y. Nuhoglu, Removal of Ni(II) ions from aqueous solutions using waste of tea factory: adsorption on a fixed-bed column, J. Hazard. Mater. B135 (2006) 328–336.
[29] O. Yavuz, Y. Altunkaynak, F. Guzel, Removal of copper, nickel, cobalt and manganese from aqueous solution by kaolinite, Water Res. 37 (2003) 948–952.
[30] E. Alvarez-Ayuso, A. Garcia-Sanchez, Removal of heavy metals from waste water by natural and Na-exchanged bentonite, Clays Clay Miner. 51 (2003) 475–480.
[31] S. Sen Gupta, K.G. Bhattacharyya, Adsorption of Ni(II) on clays, J. Colloid Interface Sci. 295 (2006) 21–32.
[32] K.G. Bhattacharyya, S. Sen Gupta, Influence of acid activation on adsorption of Ni(II) and Cu(II) on kaolinite and monmorillonite: kinetic and thermodynamic studies, Chem. Eng. J. 136 (2008) 1–13.
[33] V.K. Gupta, C.K. Jain, I. Ali, M. Sharma, V.K. Saini, Removal of cadmium and nickel from wastewater using bagasse fly ash—a sugar industry waste, Water Res. 37 (2003) 4038–4044.
[34] B. Chen, C.W. Hui, G. McKay, Film-pore diffusion modeling for the sorption of metal ions from aqueous effluents onto peat, Water Res. 35 (2001) 3345–3356.
[35] D. Satpathy, G.S. Nattarajan, Potassium bromate modification of the granular activated carbon and its effect on nickel adsorption, Adsorption 12 (2006) 147–154.
[36] J. Chen, L. Gao, J. Huang, D. Yan, Preparation of nanosized titania powder via controlled hydrolysis of titanium alkoxide, J. Mater. Sci. 31 (1996) 3497–3500.
[37] D.C. Hague, M.J. Mayo, Controlling crystallinity during processing of nanocrystalline titania, J. Am. Ceram. Soc. 77 (1994) 1957–1960.
[38] K.N.P. Kumar, J. Kumar, K. Keizer, Effect of peptization on densification and phase transformation behaviour of sol & gel derived nanostructured titania, J. Am. Ceram. Soc. 77 (1994) 1396–1400.
[39] H.K. Park, D.K. Kim, C.H. Kim, Effect of solvent on titania particle formation and morphology in thermal hydrolysis of $TiCl_4$, J. Am. Ceram. Soc. 80 (1997) 743–749.
[40] H.K. Park, Y.T. Moon, D.K. Kim, C.H. Kim, Formation of monodisperse spherical TiO_2 powders by thermal hydrolysis of $Ti(SO_4)_2$, J. Am. Ceram. Soc. 79 (1996) 2727–2732.
[41] O.H. Zhang, L. Gao, J.K. Guo, Preparation and Characterization of nanosized TiO_2 powders from aqueous $TiCl_4$ solution, Nanostruct. Mater. 11 (1999) 1293–1300.
[42] A.D. Paola, G. Cufalo, M. Addamo, M. Bellardita, R. Campostrini, R. Ischia, M. Ceccata, L. Palmisano, Photocatalytic activity of nanocrystalline TiO_2 (brookite, rutile and brookite-based) powders prepared by thermohydrolysis of $TiCl_4$ in aqueous chloride solution, Colloids Surf. A: Physicochem. Eng. Aspects 317 (2008) 366–376.
[43] J.H. Jeffery, J. Basset, J. Mendhem, R.C. Denny, Vogel's Textbook of Quantitative Chemical Analysis, 5th ed., Longman Scientific and Technical Publishers, Noida, India, 1989.
[44] G.W. Sears Jr., Determination of specific surface area of colloidal silica by titration with sodium hydroxide, Anal. Chem. 28 (1956) 1981–1983.
[45] M.B. Babic, M.J. Milovijic, B.V. Kaludierovic, Point of zero charge and intrinsic equilibrium constants of activated carbon cloth, Carbon 37 (1999) 477–481.
[46] A.V. Murugan, A.B. Gaikward, V. Samuel, V. Ravi, Preparation of nanocrystalline ferroelectric $CaBi_4Ti_4O_{15}$ by citrate gel method, Ceram. Int. 33 (2007) 569–571.
[47] S. Lagergren, Zur theorie der sogenannten adsorption geloester stoffe, Stoffe Kungliga Svenska Vetenskapskademiens, Handlingan Band 24 (1898) 1–39.
[48] Y.S. Ho, G. MacKay, A comparison of chemisorption kinetic models applied to pollutant removal on various sorbents, Trans. IChemE 76B (1998) 332–340.
[49] J.M. Chern, Y.W. Chien, Adsorption of nitrophenol onto activated carbon: isotherms and breakthrough curves, Water Res. 36 (2002) 647–655.
[50] W.J. Weber Jr., J.C. Morris, Kinetics of adsorption on carbon from solution, J. Sanit. Eng. Div. -ACSE 89 (1963) 31–59.
[51] S.J. Allen, G. Mckay, K.H.Y. Khader, Intraparticle diffusion of basic dye during adsorption onto sphagnum peat, J. Environ. Pollut. 50 (1989) 39–50.
[52] L.D. Michelsen, P.G. Gideon, E.G. Pace, L.H. Kutsal, U.S. Dept. Industry, Office of the Water Research and Technology, Bull No. 74, 1975.
[53] F. Helfferich, Ion-exchange, McGraw-Hill, New York, 1962.
[54] V.K. Kumar, V. Ramamurthi, S. Sivanesan, Modeling the mechanism involved during the sorption of methylene blue onto fly ash, J. Colloid Interface Sci. 284 (2002) 14–21.
[55] S. Wang, H. Li, Kinetic modeling and mechanism of dye adsorption on unburned carbon, Dyes Pigments 72 (2007) 308–314.
[56] S.D. Faust, O.M. Aly, Adsorption Processes for Water Treatment, Butterworth, 1987.
[57] K.H. Chu, M.A. Hashim, Kinetic studies of copper(II) and Ni(II) adsorption by oil palm ash, J. Ind. Eng. Chem. 9 (2003) 163–167.
[58] J.A. Otun, I.A. Oke, N.O. Olarinoye, D.B. Adie, C.A. Okuofu, Adsorption isotherms of Pb(II), Ni(II) and Cd(II) ions onto PES, J. Appl. Sci. 6 (2006) 2368–2376.
[59] D. Park, Y.S. Yun, K.H. Yim, J.M. Park, Effect of Ni(II) on the reduction of Cr(VI) by Ecklonia biomass, Bioresour. Technol. 97 (2006) 1592–1598.
[60] I. Villaescusa, N. Fiol, M. Martinez, N. Miralles, J. Poch, J. Serarols, Removal of copper and nickel ions from aqueous solutions by grape stalks waste, Water Res. 38 (2004) 992–1002.
[61] S.R. Shukla, R.S. Pai, Adsorption of Cu(II), Ni(II) and Zn(II) on modified jute fibres, Bioresour. Technol. 96 (2005) 1430–1438.
[62] K.G. Bhattacharyya, S. Sen Gupta, Adsorptive accumulation of Cd(II), Co(II), Cu(II), Pb(II) and Ni(II) from water on montmorillonite: influence of acid activation, J. Colloid Interface Sci. 310 (2007) 411–424.
[63] V.C. Srivastava, I.D. Mall, I.M. Mishra, Adsorption thermodynamics and isosteric heat of adsorption of toxic metal ions onto bagasse fly ash (BFA) and rice husk ash (RHA), Chem. Eng. J. 132 (2007) 267–278.
[64] Y.S. Ho, G. McKay, Competitive sorption of copper and nickel ions from aqueous solution using peat, Adsorption 5 (1999) 409–417.
[65] B. El-Eswed, F. Khalili, Adsorption of Cu(II) and Ni(II) on solid humic acid from the Azraq area, Jordan, J. Colloid Interface Sci. 299 (2006) 497–503.
[66] A.F. Ngomsik, A. Bee, J.M. Siague, V. Cabuil, G. Cote, Nickel adsorption by magnetic alginate microcapsules containing an extractant, Water Res. 40 (2006) 1848–1856.
[67] N. Boujelben, J. Bouzid, Z. Elouear, Adsorption of nickel and copper onto natural iron oxide-coated sand from aqueous solutions: study in single and binary system, J. Hazard. Mater. 163 (2009) 376–382.
[68] R.L. Tseng, S.K. Tseng, Characterization and use of high surface area activated carbons prepared from cane pith for liquid-phase adsorption, J. Hazard. Mater. B136 (2006) 671–680.
[69] A.M. El-Kamash, A.A. Zaki, M.A. El Geleel, Modeling batch kinetics and thermodynamics of zinc and cadmium ions removal from waste solutions using synthetic zeolite A, J. Hazard. Mater. 127 (2005) 211–220.
[70] B.S. Krishna, D.S.R. Murty, B.S. Jai Prakash, Thermodynamics of chromium(VI) anionic species sorption onto surfactant-modified montmorillonite clay, J. Colloid Interface Sci. 229 (2000) 230–236.
[71] A.E. Daifullah, S. Al Reffy, H. Gad, Adsorption of p-nitrophenol on inshas incinerator ash and on the pyrolysis residue of animal bones, Adv. Sci. Technol. 15 (1997) 485–496.
[72] A.S. Ozcan, S. Tunali, T. Akar, I. Kiran, Determination of the equilibrium, kinetic and thermodynamic parameters of adsorption of copper(II) ions onto seeds of capsicum annuum, J. Hazard. Mater. B124 (2005) 200–208.